# Sound scattering by several zooplankton groups. I. Experimental determination of dominant scattering mechanisms[a),b)]

Timothy K. Stanton and Dezhang Chu
*Department of Applied Ocean Physics and Engineering, Woods Hole Oceanographic Institution, Woods Hole, Massachusetts 02543-1053*

Peter H. Wiebe and Linda V. Martin
*Department of Biology, Woods Hole Oceanographic Institution, Woods Hole, Massachusetts 02543-1049*

Robert L. Eastwood
*Department of Applied Ocean Physics and Engineering, Woods Hole Oceanographic Institution, Woods Hole, Massachusetts 02543-1053*

The acoustic scattering properties of live individual zooplankton from several gross anatomical groups have been investigated. The groups involve (1) euphausiids (*Meganyctiphanes norvegica*) whose bodies behave acoustically as a fluid material, (2) gastropods (*Limacina retroversa*) whose bodies include a hard elastic shell, and (3) siphonophores (*Agalma okeni* or *elegans* and *Nanomia cara*) whose bodies contain a gas inclusion (pneumatophore). The animals were collected from ocean waters off New England (Slope Water, Georges Bank, and the Gulf of Maine). The scattering properties were measured over parts or all of the frequency range 50 kHz to 1 MHz in a laboratory-style pulse-echo setup in a large tank at sea using live fresh specimens. Individual echoes as well as averages and ping-to-ping fluctuations of repeated echoes were studied. The material type of each group is shown to strongly affect both the overall echo level and pattern of the target strength versus frequency plots. In this first article of a two-part series, the dominant scattering mechanisms of the three animal types are determined principally by examining the structure of both the frequency spectra of individual broadband echoes and the compressed pulse (time series) output. Other information is also used involving the effect on overall levels due to (1) animal orientation and (2) tissue in animals having a gas inclusion (siphonophores). The results of this first paper show that (1) the euphausiids behave as weakly scattering fluid bodies and there are major contributions from at least two parts of the body to the echo (the number of contributions depends upon angle of orientation and shape), (2) the gastropods produce echoes from the front interface and possibly from a slow-traveling circumferential (Lamb) wave, and (3) the gas inclusion of the siphonophore dominates the echoes, but the tissue plays a role in the scattering and is especially important when analyzing echoes from individual animals on a ping-by-ping basis. The results of this paper serve as the basis for the development of acoustic scattering models in the companion paper [Stanton *et al.*, J. Acoust. Soc. Am. **103**, 236–253 (1998)]. © *1998 Acoustical Society of America.* [S0001-4966(97)01010-2]

PACS numbers: 43.30.Ft, 43.30.Sf, 43.20.Fn, 43.30.Xm [JHM]

## LIST OF SYMBOLS

| | |
|---|---|
| $\alpha$ | absorption coefficient |
| $\beta_r$ | pressure-to-voltage conversion factor for receive transducer |
| $\beta_t$ | voltage-to-pressure conversion factor for transmit transducer |
| $c$ | sound speed in water |
| CP | compressed pulse output |
| $f$ | scattering amplitude |
| $f_{bs}$ | scattering amplitude in backscattering direction |
| $\gamma_g$ | amount by which the amplifier gain is reduced during calibration $[= v_t^{(s)}(\omega)/v_t^{(c)}(\omega)]$ |
| $i$ | $\sqrt{-1}$ |
| $H$ | system response of backscattering setup (not including scatterer response) |
| $k$ | acoustic wave number $(= 2\pi/\lambda)$ |
| $k_{CP}$ | normalization coefficient for compressed pulse output |
| $\lambda$ | acoustic wavelength |
| $p_{scat}$ | scattered pressure |
| $P_{inc}$ | incident pressure at the object |
| $r_c$ | distance between transducers during calibration measurement |
| $r_{ref}$ | reference distance for $\beta_t$ |
| $r_s$ | distance between source/receiver transducer pair and animal during scattering measurement |
| $\mathscr{R}_{vcal}$ | autocorrelation function of the modified calibration signal |
| $\sigma_{bs}$ | differential backscattering cross section |

---

| $\sigma$ | backscattering cross section $(=4\pi\sigma_{bs})$ |
|---|---|
| $t$ | time |
| TS | target strength |
| $v_r^{(s)}$ | receiver voltage in scattering measurement |
| $v_r^{(c)}$ | receiver voltage in calibration measurement |
| $v_t^{(s)}$ | transmitter voltage in scattering measurement |

| $v_t^{(c)}$ | transmitter voltage in calibration measurement |
|---|---|
| $\omega$ | angular frequency |
| $\langle...\rangle$ | average over ensemble of statistically independent samples |
| * | convolution |
| $\otimes$ | correlation |

## INTRODUCTION

Because of the great distances sound can travel in the water, echosounders have long been used in the remote detection and classification of marine organisms. Schools of fish quite often involve animals of similar size and the same species which makes the conversion of echo levels to abundance of animals a relatively reliable procedure (Foote and Stefánsson, 1993; MacLennan, 1990; Simmonds *et al.*, 1992). However, characterizing assemblages of zooplankton using sound generally poses a greater challenge as the assemblages quite often contain a diverse collection of animals. As the morphological properties of the zooplankton may vary from species to species (and sometimes even from animal to animal within the same species), so do the acoustic scattering properties. For example, recent laboratory studies quantitatively illustrate how the relative backscattered acoustic energy per unit animal biomass varies dramatically between the gastropods (hard elastic shell), decapod shrimp (fluidlike), siphonophores (gas bearing), and salps (fluidlike) (Stanton *et al.*, 1994a). Knowledge of this variability in scattering properties across the groups was necessary in interpreting volume reverberation levels recently observed in oceanic regions containing a mixture of species (Wiebe *et al.*, 1996).

While the study by Stanton *et al.* (1994a) confirms predictions that the overall echo levels from the zooplankters will depend strongly upon the material properties of the animals, it did not address details of the scattering signature of the animals. Much progress has been made toward describing the scattering of sound by decapod shrimp (Chu *et al.*, 1992; Stanton *et al.*, 1993a, 1993b) and euphausiids (Foote *et al.*, 1990; Chu *et al.*, 1993; Stanton *et al.*, 1993b). However, until now, little data have existed regarding other animal types, such as gastropods and siphonophores, to permit adequate acoustic characterization of those animals.

A major practical issue in modeling the scattering of sound by zooplankton is that there are thousands of species of zooplankton and a continuum of sizes present within each species. Furthermore, the scattering by the various animals depends upon the acoustic frequency and animal size, shape, orientation, and material properties. Rather than developing a different model for each size of each species (an effort that is impractical), models are being developed for animals systematically grouped according to their gross anatomical features. Such scattering models can then be developed to describe the scattering over a wide range of sizes of animals (or equivalently, a wide range of acoustic frequencies) that fit into each particular group.

In this two-paper series, the scattering properties of animals from three distinct groups are studied in depth: fluidlike (euphausiid), hard elastic shell (gastropod), and gas bearing (siphonophore) (Fig. 1). The fluidlike group is named as such because the boundary of the animal behaves acoustically as a fluid–fluid interface and does not support a shear wave (the animal actually has a thin exoskeleton surrounding the body which is being considered acoustically transparent for these applications). In this first paper, broadband measurements of acoustic backscatter by the animals are presented. The frequency spectra, compressed pulse output, and ping-to-ping variability of the echoes are analyzed. The dominant acoustic scattering properties of the animals are identified and the acoustic boundary conditions are inferred in the analysis. In the second paper, mathematical scattering models are developed based on the boundary conditions and compared with data (Stanton *et al.*, 1998). Scattering models such as these can be used to infer animal size and possibly group, as discussed in various previous studies involving inversions. See, for example, reviews on inversions of single frequency echo envelope data in Stanton and Clay (1986) and inversions of multifrequency data in Holliday and Pieper (1995), as well as recent papers on spectral classification of broadband data in Martin *et al.* (1996) and temporal classification through pulse-compression of broadband data in Chu and Stanton (submitted).

## I. BASIC EQUATIONS

The scattered pressure $p_{scat}$ is expressed in terms of the pressure $P_{inc}$ of the incident sound field as

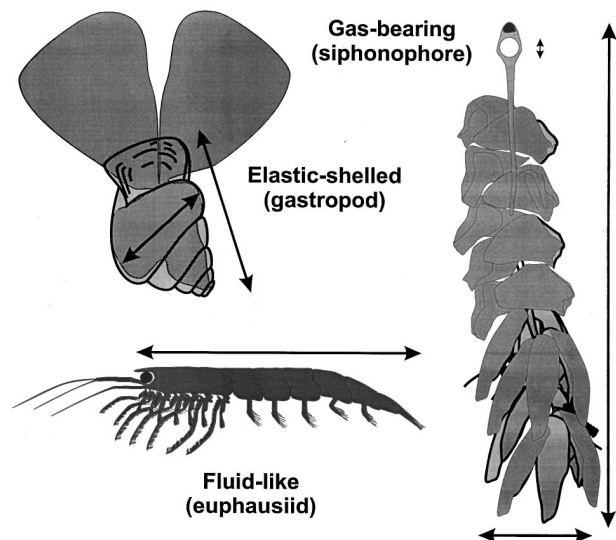$$p_{scat} = P_{inc} \frac{e^{ikr}}{r} f, \qquad (1)$$



FIG. 1. Sketches of zooplankton from several major anatomical groups. The arrows indicate parts of bodies over which various dimensions were measured.

where $f$ is the scattering amplitude of the scattered field and $r$ is the distance between the object and the receiver. This quantity $f$ indicates the efficiency to which an object scatters sound and depends upon the acoustic frequency and object size, shape, orientation, and material properties. The target strength TS is a logarithmic measure of the backscattered field (i.e., the part of the field scattered back toward the sound source) and can be expressed in terms of the scattering amplitude as

$$\text{TS} = 10 \log |f_{bs}|^2 = 10 \log \sigma_{bs}. \qquad (2)$$

Using the definition $\sigma_{bs} = |f_{bs}|^2$, the target strength was also expressed above in terms of the *differential* backscattering cross section $\sigma_{bs}$ (this differential cross section should not be confused with the commonly used backscattering cross section $\sigma$ where $\sigma = 4\pi\sigma_{bs}$). The dimensions in the above cross sections have been suppressed. The units of target strength are in decibels relative to 1 m$^2$.

The above equations pertain to single echoes. Quite often, many pings from one animal or the pings from many animals are recorded and averaged. The echoes from the individual animals at the high frequencies used to detect them tend to have random phases. As a result, the energy of the echoes from an aggregation of moving animals averaged over a number of pings is equal to the sum of the average energies of the echoes from the individual animals. Hence, it is convenient to describe the ''average'' target strength in terms of the average value of the backscattering cross section since the cross section is proportional to echo energy:

$$\langle \text{TS} \rangle = 10 \log \langle \sigma_{bs} \rangle. \qquad (3)$$

Here, the averaging process was performed on a linear scale before the logarithm was taken. The brackets $\langle \cdots \rangle$ denote the average over an ensemble of independent realizations. The average is typically over a range of animal sizes and/or orientations.

## II. EXPERIMENTAL SETUP, PROCEDURES, AND DESCRIPTIONS OF ANIMALS

We conducted a series of acoustic backscatter measurements at sea in a laboratory-style acoustic measurement tank filled with filtered seawater. The work involved catching animals from the Slope Water, Georges Bank, and the Gulf of Maine areas offshore of Cape Cod, Massachusetts, USA, and performing the scattering measurements in our 2.4-m-diam by 1.5-m-tall tank on the deck of the RV OCEANUS (1993) and RV ENDEAVOR (1994). The acoustic measurements for each animal involved a portion or all of the frequency range 50 kHz to 1 MHz. Simultaneous with the acoustic measurements in 1994, high magnification video footage of the animals was recorded. All animals were live and fresh during the measurements and were tethered so they would remain in the main beam of the transducers. In the experiments described below, data from a single euphausiid species (*Meganyctiphanes norvegica*) and gastropod species (*Limacina retroversa*) and two siphonophore species (*Agalma okeni* or *elegans* and *Nanomia cara*) were analyzed.

### A. Animals

The animals were collected with a 1-m-diam plankton net (335-$\mu$m mesh) hauled slowly and vertically from depths of 50 to 500 m. They were carefully transferred to maintenance vessels and kept alive throughout the experimental period. After acoustic data were collected, individuals were frozen for later measurements of length, wet weight, and dry weight. Other planktonic groups were also collected and used in the acoustic measurements (e.g., salps, ctenophores, and fish), but additional data are needed to accurately develop scattering models for them.

Great care was taken with the animals so that they were not exposed to air throughout the entire process of catching, sorting, examining through a microscope, tying, and deploying in and removing from the tank. This precaution was taken to prevent the possibility of bubbles attaching themselves to the animals and contaminating the measurements. Even the glue that was used in one of the tethering arrangements was applied and cured underwater. As an additional precaution the animals were gently shaken underwater to help release any bubbles that may have become attached to the animals in the process. The animals also were kept underwater in the experiment tank for a period prior to the measurements so that in case there was trapped air, it would be released from the animal or absorbed into the seawater.

Physical dimensions and weights of the animals were measured before the experiments and also sometimes after, when appropriate. Measurements of the euphausiids were straightforward. Because of the light weight of the gastropods and possible inaccuracy of direct measurement of the small millimeter-sized animals, the weights were estimated by use of the direct measurements of length and width and a published size–weight regression equation (Davis and Wiebe, 1985). The weight was sometimes used to calculate the equivalent spherical radius of the animals as a guide for scattering predictions.

The morphology of the siphonophores presented the greatest challenge in characterizing and that information presented should be considered at best approximate. When the animals were first brought onto the deck and then examined under the microscope (before the acoustic measurements took place), in several cases there were many (between two and nine) gas inclusions within the inner longitudinal tract of each animal. This is considered to be atypical and not representative of the actual morphology of the animals. These siphonophores contain only a single bubble in their natural environment (Mackie *et al.*, 1987) and the act of bringing them to the sea surface apparently caused the bubble to expand and fragment.

Once the animal was tethered in the acoustic tank, the back-and-forth sloshing of the water tended to (slightly) jerk the animal once the tether became tight at the end of each half cycle of water motion. By the end of the experiment, each animal had undergone hundreds of jerks. Upon removing each animal from the tank, it was discovered through inspection under the microscope that the gas inclusions within the animals containing multiple inclusions had not only changed position, but also quite often coalesced forming fewer or a single larger inclusion(s).

Naturally, the phenomenon of coalescing most likely had a strong effect on the measured scattering properties and definitely affected the predicted scattering properties. The

degree to which the sloshing affected the animal morphology varied from animal to animal. In some cases, the differences seemed minimal, while in several cases in 1993 only a single large gas inclusion remained. One of these latter cases, as well as animals that had a single inclusion from the initial time of capture, are studied here in detail because a single gas bubble is considered to be more typical of the animal in its natural environment. The acoustic scattering properties of a siphonophore with multiple inclusions are illustrated in Appendix A of Stanton *et al.* (1998) to illustrate the possible effects of these artifacts on the properties.

### B. Pulse-echo system

#### 1. Setup

The experimental apparatus and certain critical aspects of the data acquisition have been discussed in detail in Stanton (1990) and Chu *et al.* (1992), and summarized in Stanton *et al.* (1994a), and will only be briefly summarized here. The system involved a set of high-power single-frequency transducers: 50, 75, 120, 165, 200, 305, and 470 kHz, and 1 MHz, and a set of broadband transducers with less sensitivity, but an octave band of usable frequencies centered about the frequencies 250 kHz, 500 kHz, and 1 MHz. The transmit signals for all data in these experiments were 200 $\mu$s long. The transducers were mounted on the bottom of a 2.4-m-diam ×1.5-m-high tank, looking up at the animals that were tethered approximately 50 cm above the transducers. A pair of closely spaced identical transducers was used for each frequency or band of frequencies in the backscatter measurements. One transducer was the transmitter while the other was the receiver.

The animals were typically tethered with a combination of thin monofilament lines: a "main" line (59- or 158-$\mu$m diameter, depending on the experiment) and a secondary 59-$\mu$m-diam line. The tethers needed to be thin so that the echoes from them would be negligibly small. The euphausiids and siphonophores were tied to the main line with the secondary line, while the gastropods were glued directly to either the main or secondary line as they were too small to be tied.

The main tether was strung vertically between the midpoint of each transducer pair (even with the transducer faces) and a point out of water directly over the transducer pair. Since the tether was strung essentially parallel to the direction of acoustic transmission and backscattering, backscattering from this tether was minimized. A small loop was formed from this tether at 50-cm range from the transducers so the secondary tether could attach the animal to this main tether. The top and bottom points of the main tether were allowed to move where desired (a sliding monofilament system for the base and a moveable clip at the top) so that the animal could be easily moved horizontally over the desired transducer pair.

The two-transducer arrangement eliminated the need for a network used to isolate the transmitter signal from the receiver preamps (a circuit required in single transducer systems) and also eliminated the problem where the ringing of the transmitting transducer would interfere with the received echo at these short ranges. Furthermore, system calibration

for target strength measurements is very straightforward, as discussed later, and does not require additional hardware or a reflecting surface (this system can be calibrated at sea). A computer-based pulse-echo system was used to generate bursts of sound (tone bursts for the single frequency transducers and chirp signals for the broadband transducers) and to digitize and store each individual echo onto the computer for display and further processing.

A high-magnification underwater video camera system was also deployed in 1994 to facilitate viewing of the animal while the acoustic measurements were made. The camera was located at 50 cm above the transducers and aimed horizontally so that it was "looking" in a direction perpendicular to the direction of transmitted/backscattered acoustic waves. The directions needed to be perpendicular to enable accurate monitoring of the angle of orientation of the elongated animals relative to the direction of propagation of the acoustic signal for near broadside incidence angles where the scattered signals tend to be strongest. The video data were also stored onto tape so that the animal orientation could later be correlated with the acoustic data. The trigger signal for the acoustic ping was recorded onto the audio channel of the tape so that the correlation could be made on a ping-by-ping basis. A computer-based frame grabber, activated by the trigger signal, was used to automatically digitize video frames corresponding to acoustic pings. The digitizing was done during play back of the free running tape. For this study, the angle of orientation of one elongated animal was determined from each image by measuring the angle between the axis of the body and the main tether. With the exception of camera angle and automatic grabbing process, this method is similar to an arbitrary camera angle method described in detail in McGehee *et al.* (accepted).

The tank was filled with seawater to within 10–20 cm from the top of the tank. The at-sea measurements used water that was pumped from the ocean at the measurement site through the fire hose system of the ship and filtered with a 64-$\mu$m mesh net.

#### 2. System response, calibration, and scattering amplitude

The voltage due to the received echo in the backscattering experiment can be expressed in terms of the voltage applied to the transmit transducer, voltage-to-pressure conversion factor of the transmit transducer $\beta_t(\omega)$, pressure-to-voltage conversion factor of the receive transducer $\beta_r(\omega)$, reference distance $r_{\text{ref}}$, distance to target, phase shifts, absorption in the water, and scattering amplitude of the target as

$$v_r^{(s)}(\omega) = \underbrace{v_t^{(s)}(\omega)}_{\substack{\text{applied} \\ \text{voltage}}} \underbrace{\beta_t(\omega)\beta_r(\omega)\frac{r_{\text{ref}}\,e^{(i2\omega/c)r_s}}{r_s^2}e^{-2\alpha(\omega)r_s}}_{\substack{\text{system response} \\ H(\omega)}}$$

with $v_r^{(s)}(\omega)$ labeled *receiver voltage*.

$$\times \underbrace{f_{\text{bs}}(\omega)}_{\substack{\text{scatterer} \\ \text{response}}} \quad \text{(backscattering)}, \tag{4}$$

228    J. Acoust. Soc. Am., Vol. 103, No. 1, January 1998

Stanton *et al.*: Several zooplankton scattering. I    228

where the expression is given in the frequency domain. Although this equation is used in the context of scattering by targets that lie on the center axis (maximum response axis) of the transmit and receive transducers, $\beta_t$ and $\beta_r$ can be used to account for beampattern diffraction effects if the target is not on one or either of the center axes. Equation (4) can also be written in the time domain in terms of the convolution of the inverse Fourier transforms of the various terms on the right-hand side:

$$v_r^{(s)}(t) = v_t^{(s)}(t) * H(t) * f_{bs}(t),  \tag{5}$$

where $H(t)$ is the system *impulse* response which is the inverse Fourier transform of the system *frequency* response $H(\omega)$ (Oppenheim and Willsky, 1983). Note that the conventional notation in the signal processing literature involves upper case variables in the frequency domain and lower case variables in the time domain. Given the number of lower case terms (e.g., $f_{bs}$) in the scattering literature that are in the frequency domain, the domain here is indicated strictly by the arguments $(t)$ and $(\omega)$. For example, $v_r^{(s)}(t)$ is the inverse Fourier transform of $v_r^{(s)}(\omega)$, etc.

In order to determine transducer efficiencies in the system response term $H$, the system is calibrated by separating the transducers, aiming them toward each other, and measuring signals as a result of the acoustic pulse traveling along the direct path between the two. With the target removed from the scattering region, the measurement is performed in a manner similar to that of the scattering experiment, but with the transmitter voltage greatly reduced to prevent saturation of the receiver preamps. During calibration, it was obvious that the response of the broadband transducers was not uniform across the band. The normalization process in the calibration procedure removed any nonuniformity. The system was calibrated at the beginning and end of each cruise. The spectrum of the receiver voltage in this calibration setup is

$$v_r^{(c)}(\omega) = v_t^{(c)}(\omega) \beta_t(\omega) \beta_r(\omega) \frac{r_{\text{ref}}}{r_c}$$
$$\times e^{(i\omega/c)r_c} e^{-\alpha(\omega)r_c} \quad \text{(calibration)},  \tag{6}$$

where the superscript $(c)$ denotes calibration voltages.

Equation (4) shows that only the product of the transmit and receive transducer factors is required to relate the receiver voltage to the scattering amplitude rather than those quantities separately. Rearranging the terms in Eq. (6), the product can be written as

$$\beta_t(\omega) \beta_r(\omega) = \frac{v_r^{(c)}(\omega)}{v_t^{(c)}(\omega)} \frac{r_c}{r_{\text{ref}}} e^{-(i\omega/c)r_c} e^{\alpha(\omega)r_c}.  \tag{7}$$

Inserting this expression for the product directly into Eq. (4) gives the following equation for the spectrum of the receiver voltage:

$$v_r^{(s)}(\omega) = \frac{v_t^{(s)}(\omega)}{v_t^{(c)}(\omega)} \frac{r_c}{r_s^2} e^{(i\omega/c)(2r_s - r_c)} e^{-\alpha(\omega)(2r_s - r_c)}$$
$$\times v_r^{(c)}(\omega) f_{bs}(\omega)  \tag{8}$$
$$= \gamma_g(\omega) \frac{r_c}{r_s^2} e^{(i\omega/c)(2r_s - r_c)} e^{-\alpha(\omega)(2r_s - r_c)}$$
$$\times v_r^{(c)}(\omega) f_{bs}(\omega),  \tag{9}$$

where now the receiver voltage in the scattering experiment is expressed in terms of voltage spectra from both the scattering and calibration measurements. For convenience, the term $\gamma_g(\omega) \equiv v_t^{(s)}(\omega)/v_t^{(c)}(\omega)$ is defined as the ratio of the transmitter voltage spectra in the two types of measurements. In the cases where the reduction in transmitter voltage for the calibration experiment is uniform across the frequency band, then $\gamma_g$ is a constant.

As with Eq. (5) the convolution operator can be used to write the above equation in the time domain:

$$v_r^{(s)}(t) = s(t) * v_r^{(c)}(t) * f_{bs}(t),  \tag{10}$$

where $s(t)$ is the inverse Fourier transform of

$$s(\omega) \equiv \gamma_g(\omega) \frac{r_c}{r_s^2} e^{(i\omega/c)(2r_s - r_c)} e^{-\alpha(\omega)(2r_s - r_c)}.  \tag{11}$$

In Eq. (10) the receiver voltage time series in the scattering experiment is expressed in terms of the convolution of the system term, $s(t)$, with the received voltage time series in the calibration experiment and inverse Fourier transform of the scattering amplitude. Rearranging Eq. (9) and using the definition of $s(\omega)$ results in the following expression for the scattering amplitude of the target in terms of the various terms from the scattering and calibration experiments:

$$f_{bs}(\omega) = \frac{v_r^{(s)}(\omega)}{s(\omega) v_r^{(c)}(\omega)}.  \tag{12}$$

Aside from the system term $s(\omega)$, the scattering amplitude is shown to be related to the receiver voltage from the scattering experiment normalized by the receiver voltage from the calibration measurement. It is the above expression that is used to calculate target strength versus frequency according to Eq. (2). While Eq. (12) is written in general form, it simplifies in the following cases: (1) When $\gamma_g(\omega)$ is constant in the band of interest (see above discussion) and the frequencies are low enough or $2r_s = r_c$, then $|s(\omega)|$ is independent of frequency. (2) For narrowband transducers, the various terms are quite often evaluated in terms of the envelope levels of their signals.

For both cases, it is advantageous to set up the experiment so that $2r_s = r_c$. With $2r_s - r_c = 0$ in the exponent of the attenuation term in $s(\omega)$, it is not required to know the attenuation coefficient of the water and

$$s = \gamma_g r_c / r_s^2,  \tag{13}$$

where now the frequency dependence of $\gamma_g$ has been removed. Here, $r_s$ and $r_c$ are still both given explicitly to account for cases in which $r_c \neq 2r_s$ and effects due to attenuation and phase shifts are not important.

### 3. Pulse compression processing

Pulse compression techniques are applied to the time series of the receiver voltage in the scattering experiment in order to both enhance the signal-to-noise ratio as well as to help determine some of the underlying physical mechanisms of the scattering processes. Pulse compression processing, which involves cross-correlating the received voltage with the transmit signal waveform, is generally very useful for detection of a broadband signal in the presence of noise as it

will tend to compress the signal to a short, higher level signal with a duration comparable to the inverse bandwidth of the signal (Skudrzyk, 1971; Turin, 1960; Winder and Loda, 1981). Uncorrelated noise in this case is not enhanced from the process and the signal-to-noise ratio is subsequently increased as a result of the filtering. In fact, it has been proven that when the signal component of the received voltage is identical (or proportional) to the transmitted wave form, then the pulse compression process maximizes the signal-to-noise ratio (this special case is referred to as a *matched* filter). For traditional detection of a signal in the presence of noise, the noisy signal is cross correlated with the original (noiseless) signal, which produces a signal resembling the autocorrelation function of the original signal (in the absence of noise, the result is exactly equal to the autocorrelation function).

In the scattering experiment, the (noiseless) ''signal'' (or ''replicate'') ideally would be the convolution of the applied signal with the known response of the system and the scattering amplitude of the target which is typically unknown. With an unknown scattering amplitude, it is not possible then to form the true signal or replicate. Hence, the filter cannot truly match the signal. In order to perform pulse compression processing of the signals in this scattering experiment, the replicate is constructed from the case resembling ideal scattering—that is, the scattering amplitude used in the convolution in Eq. (10) is uniform over all frequencies (e.g., such as with a perfectly reflecting wall). In practice, this replicate is the received voltage in the bistatic calibration when the transducers are facing each other. Applying this replicate when processing echoes from a real target will result in deviations from the matched filter output from the idealized ''expected'' case, due to deviations of the scatterer from the idealized target. These deviations contain useful information on the boundary conditions of the animals as will be shown in later sections.

The expression for the compressed pulse output is determined by using all components of Eq. (10) except for the scattering amplitude for the replicate:

$$CP(t) = k_{CP} \, v_r^{(s)}(t) \otimes v_r^{(c)'}(t), \tag{14}$$

where $v_r^{(s)}(t)$ is the measured noisy signal and the replicate $v_r^{(c)'}(t)$ is a filtered and scaled version of the receiver voltage in the calibration experiment:

$$v_r^{(c)'}(t) = s(t) * v_r^{(c)}(t) \tag{15}$$

(see above discussions for simplification of $s$). Equation (14) is a true matched filter only for the case of an ideal reflector where $f(\omega) = 1$ [i.e., $f(t) = \delta(t)$ where $\delta(t)$ is the delta function]. In that ideal case, beginning with Eq. (10): $v_r^{(s)}(t) = s(t) * v_r^{(c)}(t) * f_{bs}(t) = s(t) * v_r^{(c)}(t) * \delta(t) = s(t) * v_r^{(c)}(t) \equiv v_r^{(c)'}(t)$, hence making $v_r^{(c)'}(t)$ a true replicate. When real scatterers are involved, deviations in the compressed pulse output from the idealized (matched filter) case provide information on the target scattering amplitude $f(t)$. Note also that the cross correlation process in Eq. (14) is equivalent to (1) the convolution between one of the time series and the time-reversed time series of the other and (2) the inverse Fourier transform of the product of the spectrum of one signal and

the complex conjugate (corresponding to time-reversal) of the spectrum of the other signal (Skudrzyk, 1971).

The normalization coefficient is equal to the inverse of the autocorrelation function of the modified calibration receiver voltage evaluated at the maximum point ($t=0$):

$$k_{CP} = R_{vcal}^{-1}(0), \tag{16}$$

where the autocorrelation function of $v_r^{(c)'}(t)$ is defined as

$$R_{vcal}(t) \equiv v_r^{(c)'}(t) \otimes v_r^{(c)'}(t). \tag{17}$$

Substituting expressions for $k_{CP}$ from Eq. (16) and $v_r^{(s)}(t)$ from Eq. (10) into Eq. (14) and using Eq. (15) and the relations $s_1 * s_2 = s_2 * s_1$ and $(s_1 * s_2) \otimes s_3 = s_1 \otimes (s_2 \otimes s_3)$ gives

$$CP(t) = f_{bs}(t) \otimes \frac{R_{vcal}(t)}{R_{vcal}(0)} \tag{18}$$

[see, for example, Appendix B of Chu and Stanton (submitted) for a derivation of the latter above identities involving $s_1$, $s_2$, and $s_3$].

This expression shows the compressed pulse output to be equal to the scattering amplitude of the target cross correlated with the normalized autocorrelation function of the modified calibration signal. This output is very useful in analyzing the scattering by targets. For a target with only one dominant scattering feature, the compressed pulse output due to an incident chirp signal will resemble a sinc function time series. For a target with multiple scattering features, the output will resemble a series of sinc functions with different time delays and amplitudes according to the relative location and scattering amplitudes of the individual features, respectively. The above equation will be used to extract fundamental scattering information from the time series of the echoes from the animals. A much more extensive treatment of pulse compression techniques and application to the zooplankton scattering problem is presented in Chu and Stanton (submitted).

## III. RESULTS

### A. Data quality

A great challenge in the experiments involved the contaminants in the data. With most target strengths below about $-70$ dB, there were several sources of contamination in the data with comparable equivalent target strength levels. As with any system, self noise (electrical in this case) was one limiting factor. The (self-) noise floor of the broadband transducers was roughly $-90$ to $-85$ dB in a given spectral bin. The floor of the narrowband transducers was usually well below $-90$ dB. In addition to electrical self-noise, there were several sources of unwanted echoes: 1) Echoes from the surrounding walls of the tank and mounts. These echoes were stable in time and were generally not a problem as they were digitally removed in real-time with the oscilloscope. 2) Echoes from the tether of the animal. The target strength of too large of a tether can sometimes be comparable to or greater than the target strength of the animal. Great effort was made to ensure that the tether had a target strength much lower than that of the animal. Since the thinnest tethers (thinner than human hair) were so difficult to handle, they were

usually used only with the animals with the lowest target strength. Thicker tethers were used with animals that had higher target strengths. 3) Echoes from the glue that was sometimes used to attach the tether to the animal. When the animal was so small that a tether could not be tied around it, the tether needed to be glued to the animal. Sometimes the echoes from the glue dominated the overall echoes and those data were discarded. Great effort was made to minimize the use of glue as well as to minimize the amount of glue applied when it was used. 4) Echoes from other parts of the water volume. Reverberation from the water from near the animal degraded many sets of data. This reverberation was associated with the turbulent motion of the water due to ship motion. It was present when the water was sloshing back and forth and tended to disappear when the tank was still (for example, on calm nights when the ship was moving slowly downwind). The reverberation tended to be stronger at the lower frequencies.

Tether target strengths as low as −95 dB at 200 kHz were achieved during calm sea conditions. Tether plus glue target strengths lower than about −85 dB with the 500-kHz broadband transducers could be achieved with the right combination of tether and small application of glue. The reverberation associated with the motion of the tank easily reached levels of about −70 dB for certain sea conditions.

Because of the above sources of contamination, the data were examined with great scrutiny both during the time of experimentation as well as afterward. Generally, the single ping analysis was affected the most by the contamination as any source of unwanted signal would tend to alter the structure of the target strength versus frequency curves (see the Appendix). Hence, only a minority of data is usable for the single ping analysis where the precise structure of the TS curves is examined. However, for examination of echoes averaged over many pings, the criteria for selection were not as strict and far more data are usable. As long as the target echo was at least about 6 dB greater than the level of the unwanted echo, averages could be calculated with reasonable accuracy.

## B. Single ping echoes

Because of the relatively high quality of data (a combination of signal-to-noise ratio and bandwidth) coming from the broadband 500-kHz transducers, the spectral nature of the scattering as measured from those transducers is analyzed on an individual ping basis. The scattering measurements over the ∼400 to 650-kHz band showed significant structure in most target strength versus frequency plots for the euphausiids and a significant fraction of the pings for the gastropods and siphonophores (Fig. 2). In the case of the gastropods and siphonophores, there are also many pings where the variability in the spectra was small and random. A small fraction of data from the euphausiids also exhibited low variability in the spectra. Each of the echoes recorded from the 500-kHz broadband transducers from the euphausiid typically showed a series of peaks and dips (or nulls), some mostly regularly spaced and others mostly irregularly spaced. Since some of the nulls dip below the noise/unwanted reverberation level of the system, it is expected that the lowest part of the nulls are affected accordingly. The
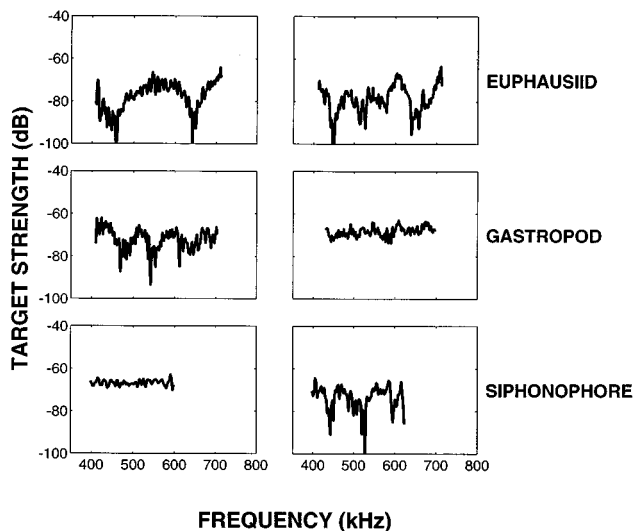


FIG. 2. Target strength versus frequency for two individual pings (left/right panel), each from single zooplankters. Since the euphausiid and siphonophore were allowed to change orientation throughout the ping sequence, two (nonconsecutive) pings from the same animal were selected in each case to illustrate ping-to-ping variability. The gastropods remained nearly fixed at a random orientation and one ping each from two same-size animals were selected to illustrate variability. Species and lengths of the animals are, euphausiid: *Meganyctiphanes norvegica*, 34 mm; gastropod: *Limacina retroversa*, 2 mm; siphonophore: *Agalma okeni* or *elegans*, 48 mm (gas inclusion is 1.3 mm long by 0.5 mm wide).

Fourier component of the noise that is at or near the null will tend to shift the position of the null. The target strength pattern, even when regular and with a high signal-to-noise ratio, tended to shift randomly from ping-to-ping—a phenomenon also observed with broadband echoes from decapod shrimp (Chu *et al.*, 1992). The euphausiid was tethered in such a way (around its mid-section) that it was free to change orientation over the entire range of angles (Fig. 3) and significant variability in the type of pattern is expected.
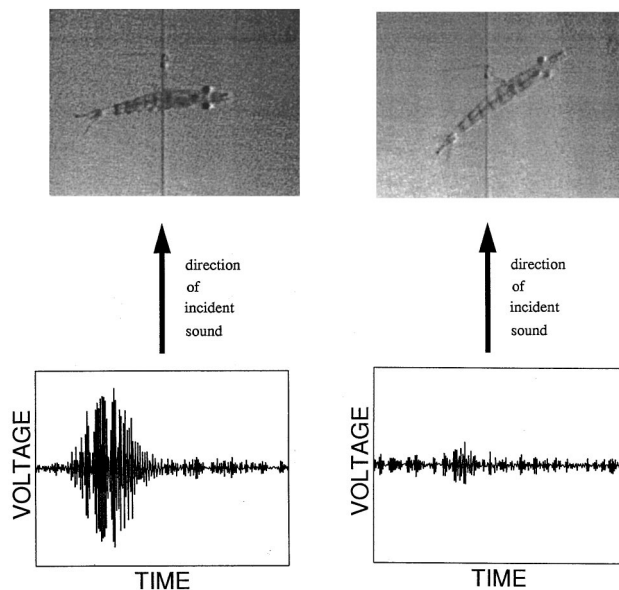


FIG. 3. Illustration of orientation effects of the backscattering by a 36-mm-long euphausiid (*Meganyctiphanes norvegica*). The video image was captured to within one frame (∼33 ms) of the time the 500-kHz broadband signal was transmitted.
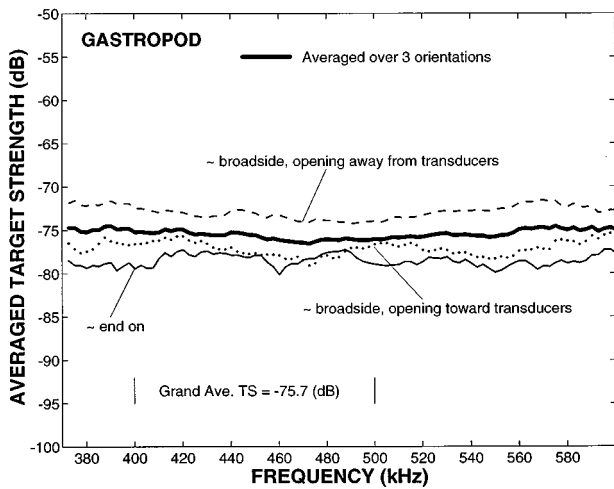
FIG. 4. Target strength versus frequency from averages over hundreds of pings for a single gastropod in each of three different orientations. The thick line corresponds to an unweighted average of the average levels from each orientation. All averages performed on a linear scale before the logarithm is taken. The gastropod (*Limacina retroversa*) was 1.5 mm long.
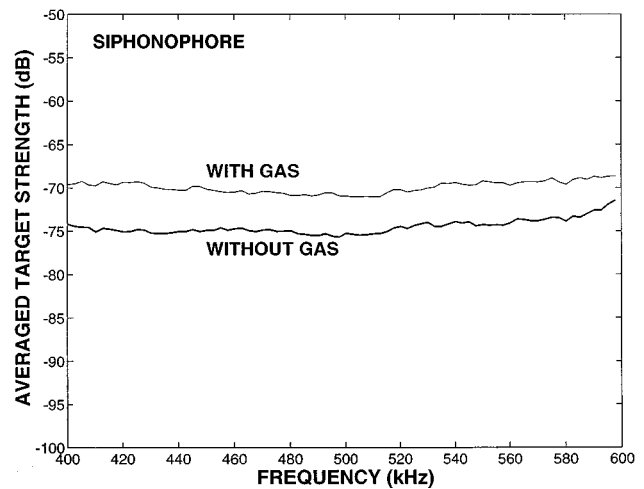


FIG. 5. Target strength versus frequency from averages over hundreds of pings for a siphonophore with and without its pneumatophore. Average performed on a linear scale before logarithm was taken. Same animal as in Fig. 2.

Similarly, the siphonophore was tethered in such a way (near its pneumatophore) which allowed much freedom of movement and, in turn, much ping-to-ping variability in the pattern. Because of the small size of the gastropods and the fact that they were not trying to swim during the experiments, they did not move much, if at all, and demonstrated relatively consistent patterns from ping to ping for a given animal.

## C. Orientation effects

The effects of orientation (as determined by high-magnification video footage) on the scattering by the euphausiids were quite noticeable (Fig. 3). While the animal was near broadside incidence, the echo levels were, on the average, relatively high, although there was significant variability in the level from ping to ping. Off broadside incidence, the echo levels were generally much lower. The scattering by the siphonophores tended to remain relatively high regardless of orientation and there tended to be variability in the level from ping to ping. The gastropod data also demonstrated an orientation dependence. Since the orientation of the animals tended to be relatively fixed throughout a ping sequence, a large number of pings could be collected and averaged for a given orientation angle.

In one series of gastropod experiments, three orientation angles were studied for a single animal: one in which the opercular opening of the animal was facing away from the transducers (with body axis near broadside incidence), one in which the opening was facing toward the transducers (with body axis about 30° off broadside incidence), and one in which the opening was facing perpendicular to the propagation of the incident sound waves with the apex of the animal aimed toward the transducers (i.e., ''end-on''). The average target strength values varied over a range of about 5 dB over the range of orientation angles (Fig. 4). The broadside orientation in which the opercular opening was facing away from

the transducers resulted in the highest values of target strength.

## D. Removal of gas inclusion from siphonophore

In order to further investigate the dominant scattering mechanisms of the siphonophores, the target strength was measured for one animal for a series of pings first as a whole (undissected) animal, and then with the pneumatophore removed (the animal remained alive after the pneumatophore was removed) (Fig. 5). The target strengths, averaged over the various 200-ping series, showed a significant drop in level of roughly 5 dB once the pneumatophore was removed. The statistics of the echo envelopes of the animal with and without the gas also showed a change in shape and average level (Fig. 6). The shape of the PDF (at 560 kHz) associated
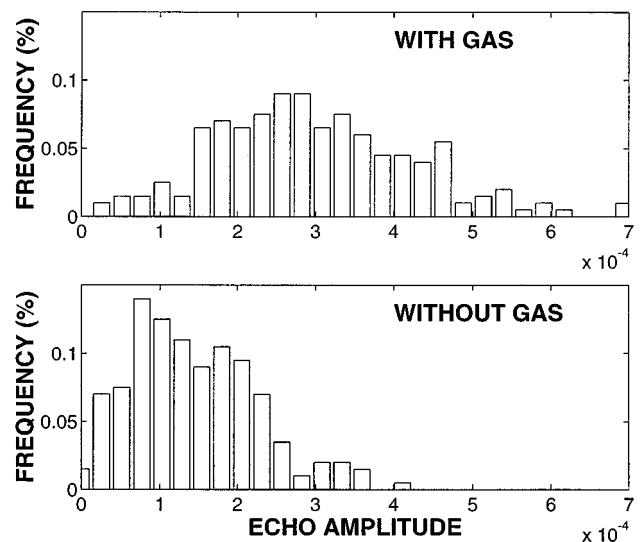


FIG. 6. Echo envelope histograms of siphonophore from Fig. 5 with and without its pneumatophore. Echo amplitude is $|f_{bs}|$ expressed in units of meters. Data from 560-kHz Fourier bin of 500-kHz broadband echo. Here, 200 echoes per plot are used to form the histograms.
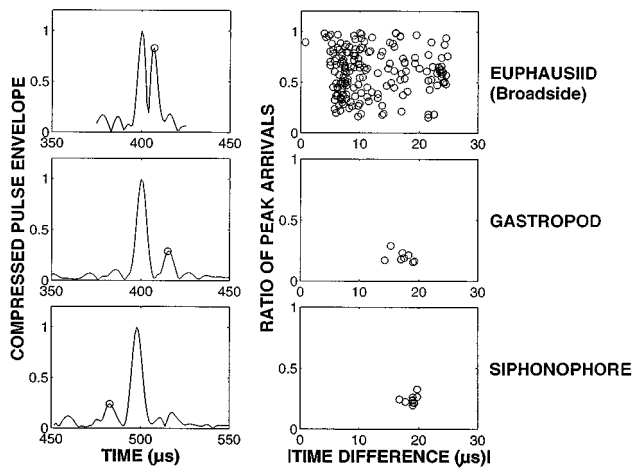
FIG. 7. Envelope of compressed pulse output of a single ping (left column) and statistics (right column) of secondary arrival from each of the three animal types. The 200-$\mu$s-long echoes were compressed to about 10-$\mu$s-long through cross correlation with the calibration waveform. This process allows certain features of the animals to be resolved acoustically. Examples of secondary arrivals are indicated by circled peaks in left column. The ratio of the amplitude of the secondary arrival to the amplitude of the principal arrival for various pings is given in the right column. The secondary return arrived after the principal arrival for the euphausiid and gastropod and before for the siphonophore. The euphausiid was very near broadside (dorsal) incidence for the example ping in the left plot. For the entire ping series shown in the plot on the right, the euphausiid was generally near broadside (dorsal) incidence with occasional exceptions. The main body of the siphonophore is closer to the transducer than the gas for the selected ping series. Species and lengths of animals are, euphausiid: same animal as in Fig. 3; gastropod, same animal as in Fig. 4; siphonophore: *Nanomia cara*, 26 mm (gas inclusion was 1.5 mm long by 1 mm wide). Absolute value of time difference given on right side because siphonophore values are all negative for this particular ping sequence.

with the whole animal tends to be Gaussian-like while the shape of the PDF of the body-only animal appears Rayleigh-like.

### E. Statistics of secondary arrivals

In addition to examining the spectral content of individual pings, the envelope of the compressed pulse output of
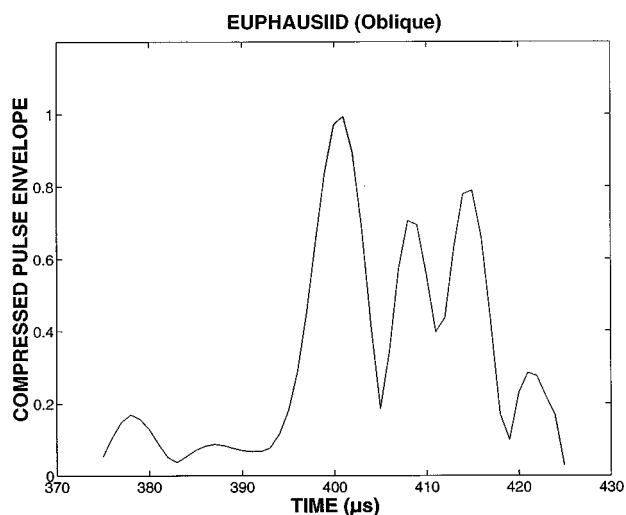


FIG. 8. Envelope of compressed pulse output of a single echo from a euphausiid near head-on incidence. Same animal as in Fig. 7.

the time series of the individual pings was also studied (Figs. 7 and 8). The compressed pulse output showed typically more than one main lobe. The level of each ''secondary'' main lobe was usually lower than that of the ''principal'' main lobe but higher than the sidelobes of the principal main lobe that would be artifacts of the signal processing. The statistics of the relative amplitude and time of arrival of the secondary main lobes were also studied using the highest quality echoes (i.e., least contamination due to noise and reverberation) for each animal (right column of Fig. 7). In the euphausiid data, there were typically two main peaks when the animal was oriented near broadside (Fig. 7) and quite often more than two peaks once the animal was well away from broadside (Fig. 8). The statistical analysis for euphausiids in Fig. 7 involved just the near-broadside echoes.

## IV. DISCUSSION

Most data indicate that there are scattering returns coming in from more than one part of the body: (1) Frequency domain: the pattern of the target strength versus frequency curves quite often had a series of peaks and nulls. This type of pattern is similar to that of an optical interferometer in which light waves experience multiple bounces and interfere upon exiting the device. The position of the peaks and nulls depends upon a combination of optical wavelength and separation between the mirrors. For the animals, a similar argument may hold as the interference patterns imply that there are echoes (at least two) coming from different parts of the body and are interfering according to the acoustic wavelength and separation between the scatterers (or more generally, the total path length experienced by each echo). (2) Time domain: the compressed pulse output shows that the echoes from the animals typically possessed more than one highlight, indicating that more than one part of the animal is contributing to the echo. Sometimes the secondary arrivals were not large enough to cause an oscillatory pattern in the target strength versus frequency curve (not shown). (3) In addition to the spectral and temporal studies of all animals, examination of the siphonophore data before and after the gas inclusion was removed indicated clearly that, although the gas contributes significantly to the echo, the tissue cannot be ignored under some conditions.

The broadest separation between nulls in the target strength versus frequency curve for the euphausiid was consistent with receiving echoes from the front and back body walls of the animal at broadside incidence. This observation is consistent with the data collected involving decapod shrimp by Chu *et al.* (1992). The closer separations between the nulls are consistent with distances greater than the (cylindrical) diameter of the animal, which is consistent with the animal being off broadside (in the extreme case of end-on, it is possible that echoes could be separated by a distance equal to the length of the animal). The compressed pulse output was not able to resolve individual echoes when the separation between the nulls was the largest (i.e., a single main lobe in the output was observed). When the separation between the nulls was slightly smaller, two main lobes were

resolved with temporal spacing consistent with distances slightly larger than the diameter of the animal.

While some patterns of target strength versus frequency were regular (implying that there were only two major sources of scattering per euphausiid), other patterns for the same animal were quite irregular. As shown in Stanton *et al.* (1994b) with decapod shrimp, there can be at least six major sources of scattering in that case. It is hypothesized that once the animal is away from broadside incidence and/or possibly configured in an irregular shape, then other parts of the body will also contribute significantly to the scattering. Hence, at least two sources of scattering must be modeled for the euphausiid and possibly more.

The data analyzed for the siphonophore indicate that the scattering is due to a combination of the gas and surrounding tissue. The separation between the main lobes of the compressed pulse output for the siphonophore data is consistent with distances comparable to the length of the siphonophore. While the gas is shown to dominate the average target strength levels, the tissue apparently plays a role in the pattern of target strength versus frequency for single ping data. If the tissue contributed a negligible amount, then the pattern would be flat. For a fraction of the pings, the pattern was flat, indicating that the variable echo from the tissue did not contribute during those pings. However, when the patterns were irregular, the echo from the tissue in these realizations may have been large enough (i.e., on the tail of the echo envelope PDF) to interfere with the echo from the gas.

While the various patterns of data for the euphausiids and siphonophores are consistent with two-way paths due to scattering from different parts of the animal bodies, the patterns for the gastropods are not consistent with separations of any dimension of the body. In fact, the oscillatory pattern of target strength versus frequency for the gastropod contains a null separation consistent with a fluidlike animal diameter of approximately 10 mm. Because the gastropods were about 1 mm$\times$2 mm in size, it is apparent that another scattering mechanism must be contributing to the echo: A thin but hard elastic shell may not allow waves to significantly penetrate into the body and reflect back to interfere with the echo from the front interface. However, it is possible that the elastic shell is supporting a circumferential wave. One strong candidate is the zeroth-order antisymmetric Lamb wave (i.e., $a_0$ or flexural wave). It is quite strong and travels at subsonic speeds in this range of $ka$ (near unity). If one were to use one-half the circumference of the shell as its travel path, then the 75-kHz null spacing would be consistent with the interference between the echo from the front interface of the shell and a Lamb wave traveling at about $\frac{1}{8}$ that of the speed of sound in water. This subsonic speed is within a reasonable range of expected values for thin shells and near unity values of $ka$ (see, for example, Kargl and Marston, 1989; Kaduchak *et al.*, 1995). The hypothesis of the animal shell supporting a Lamb wave is consistent with the appearance and disappearance of the interference pattern in the target strength versus frequency curve for single pings. It is possible that the animal can be oriented in such a way that the opercular opening can stop the propagation of the Lamb waves, hence only the echo from the front interface would remain with no interference.

## V. CONCLUSIONS

In conclusion, through a series of controlled laboratory studies, key scattering mechanisms of several types of zooplankton have been inferred acoustically. The data indicate that scattering is typically due to more than one part of the body. The euphausiid (a fluidlike animal) gives rise to at least two echoes. When broadside, the echoes are due to arrivals from the front and back interfaces (body walls) of the animal. The gas inclusion of the siphonophore (a gas-bearing, fluidlike body) dominates the overall levels of the scattering, but the tissue can play a role, especially when analyzing data on a ping-by-ping basis. The gastropod (elastic-shelled animal) gives rise to echoes from the front interface and possibly a slow-traveling circumferential (Lamb) wave. These scattering mechanisms will be taken into account in the companion paper (Stanton *et al.*, 1998) in the formulation of mathematical scattering models.

## APPENDIX: CONTAMINATION OF ECHO DATA DUE TO TURBULENT WATER VOLUME

There was scattering from the water volume associated with the water motion. The greater the motion, the greater the level of scattering. Although no controlled study was performed to determine the source of the reverberation, one possible source could be salinity and temperature microstructure (Stanton *et al.*, 1994b; Seim *et al.*, 1995). If that were the case, the salinity and temperature microstructure would give rise to a sound velocity microstructure which, in turn, would diffusely scatter the incident acoustic field. Regardless of the source of reverberation, it occurred frequently enough that it had to be taken into account in the identification of valid data.

The scattering from the turbulent water volume surrounding the animal quite often dramatically affected the pattern of curves of the target strength versus frequency from individual pings. As a result of this observation, single pings
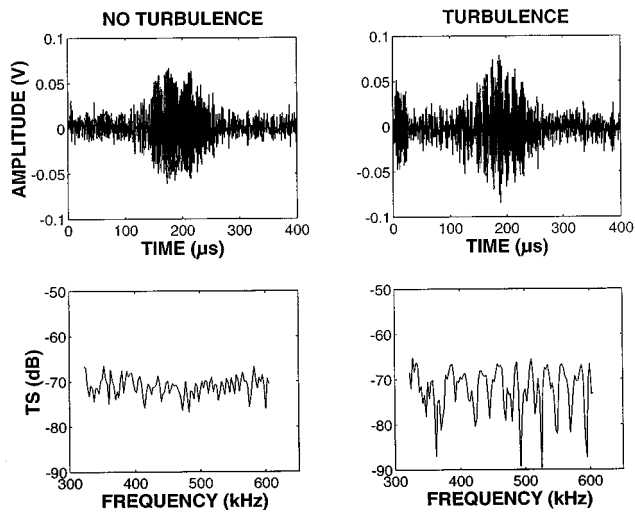
**NO TURBULENCE**      **TURBULENCE**

FIG. A1. Time series and target strength versus frequency for single echoes from a siphonophore with and without the presence of local volume reverberation associated with turbulence. Same animal as in Fig. 7. Left column shows echo due to animal with apparently no turbulence. Right column shows echo due to animal with turbulence echo explicitly appearing at leftmost part of time series. Deep rapid oscillations in TS pattern occurred (lower right) even with the (visible) turbulence echo gated out, indicating presence of another turbulence echo occurring during time of animal echo. The leading and trailing edges of the 200-$\mu$s-long waveforms are below the noise level in the time series.

that were selected for detailed analysis were chosen with great scrutiny. Those that were selected for single ping analysis must have been part of a series of pings where there was no apparent background reverberation activity for several pings before and after (both raw time series and compressed pulse output were used in the examinations). Only then was there confidence that there was little or no contamination of the animal echo due to volume reverberation from turbulence.

The turbulence effects could be seen in the time series as an irregular short-lived echo appearing at times not corresponding to the location of the animal (left-most echo in turbulence time series in top right-hand plot in Fig. A1). In the sampling window of the data acquisition system, the background echoes could be observed before, during, and/or after the echo from the animal. The resultant pattern of target strength versus frequency curve sometimes contained deep rapid oscillations, departing from the slower oscillations or even relatively flat curves observed when reverberation was apparently not present (Fig. A1). The target strength pattern was sometimes oscillatory even when a turbulence echo apparent in the time series was gated out. Evidently, there was another turbulence echo arriving at nearly the same time as that from the animal. In that case, this other echo could not be gated out.

Chu, D., and Stanton, T. K. (**submitted**). ''Application of pulse compression techniques to broadband acoustic scattering by individual marine organisms,'' submitted to J. Acoust. Soc. Am.

Chu, D., Foote, K. G., and Stanton, T. K. (**1993**). ''Further analysis of target strength measurements of Antarctic krill at 38 and 120 kHz: Comparison with deformed cylinder model and inference of orientation distribution,'' J. Acoust. Soc. Am. **93**, 2985–2988.

Chu, D., Stanton, T. K., and Wiebe, P. H. (**1992**). ''Frequency Dependence

of Sound Backscattering from Live Individual Zooplankton,'' ICES J. Mar. Sci. **49**, 97–106.

Davis, C., and Wiebe, P. (**1985**). ''Macrozooplankton Biomass in a Warm-Core Gulf Stream Ring: Time Series Changes in Size, Structure, and Taxonomic Composition and Vertical Distribution,'' J. Geophys. Res. **90**, 8871–8884.

Foote, K. G., and Stefánsson, G. (**1993**). ''Definition of the Problem of Estimating Fish Abundance Over an Area from Acoustic Line-Transect Measurements of Density,'' ICES J. Mar. Sci. **50**, 369–381.

Foote, K. G., Everson, I., Watkins, J. L., and Bone, D. G. (**1990**). ''Target strengths of Antarctic krill (*Euphausia superba*) at 38 and 120 kHz,'' J. Acoust. Soc. Am. **87**, 16–24.

Holliday, D. V., and Pieper, R. E. (**1995**). ''Bioacoustical Oceanography at High Frequencies,'' ICES J. Mar. Sci. **52**, 279–296.

Kaduchak, G., Kwiatkowski, C. S., and Marston, P. L. (**1995**). ''Measurement and interpretation of the impulse response for backscattering by a thin spherical shell using a broad-bandwidth source that is nearly acoustically transparent,'' J. Acoust. Soc. Am. **97**, 2699–2708.

Kargl, S. G., and Marston, P. L. (**1989**). ''Observations and modeling of the backscattering of short tone bursts from a spherical shell: Lamb wave echoes, glory, and axial reverberations,'' J. Acoust. Soc. Am. **85**, 1014–1028.

Mackie, G. O., Pugh, P. R., and Purcell, J. E. (**1987**). ''Siphonophore Biology,'' Adv. Mar. Sci. **24**, 97–111.

MacLennan, D. N. (**1990**). ''Acoustic measurement of fish abundance,'' J. Acoust. Soc. Am. **87**, 1–15.

Martin, L. V., Stanton, T. K., Wiebe, P. H., and Lynch, J. F. (**1996**). ''Acoustic Classification of Zooplankton,'' ICES J. Mar. Sci. **53**, 217–224.

McGehee, D. E., O'Driscoll, R. L., and Martin Traykovskii, L. V., ''Effects of orientation on acoustic scattering for Antarctic krill at 120 kHz,'' Deep Sea Research (accepted).

Oppenheim, A. V., and Willsky, A. S. (**1983**). *Signals and Systems* (Prentice–Hall, London).

Seim, H. E., Gregg, M. C., and Miyamoto, R. T. (**1995**). ''Acoustic Backscatter from Turbulent Microstructure,'' J. Atmos. Ocean. Tech. **12**, 367–380.

Simmonds, E. J., Williamson, N. J., Gerlotto, G., and Aglen, S. (**1992**). ''Acoustic Survey Design and Analysis Procedure: A Comprehensive Review of Current Practice,'' ICES Cooperative Research Report No. 187. International Council for the Exploration of the Sea. Palaegrade 2-4, DK-1261, Copenhagen K, Denmark.

Skudrzyk, E. (**1971**). *The Foundations of Acoustics* (Springer-Verlag, New York).

Stanton, T. K. (**1990**). ''Sound scattering by spherical and elongated shelled bodies,'' J. Acoust. Soc. Am. **88**, 1619–1633.

Stanton, T. K., and Clay, C. S. (**1986**). ''Sonar Echo Statistics as a Remote-Sensing Tool: Volume and Seafloor,'' IEEE J. Ocean Eng. **OE-11**, 79–96.

Stanton, T. K., Chu, D., and Wiebe, P. H. (**1998**). ''Sound scattering by several zooplankton groups. II. Scattering models,'' J. Acoust. Soc. Am. **103**, 236–253.

Stanton, T. K., Clay, C. S., and Chu, D. (**1993a**). ''Ray representation of sound scattering by weakly scattering deformed fluid cylinders: Simple physics and application to zooplankton,'' J. Acoust. Soc. Am. **94**, 3454–3462.

Stanton, T. K., Chu, D., Wiebe, P. H., and Clay, C. S. (**1993b**). ''Average echoes from randomly oriented random-length finite cylinders: Zooplankton models,'' J. Acoust. Soc. Am. **94**, 3463–3472.

Stanton, T. K., Wiebe, P. H., Chu, D., and Goodman, L. (**1994b**). ''Acoustic Characterization and Discrimination of Marine Zooplankton and Turbulence,'' ICES J. Mar. Sci. **51** 469–479.

Stanton, T. K., Wiebe, P. H., Chu, D., Benfield, M., Scanlon, L., Martin, L., and Eastwood, R. L. (**1994a**). ''On Acoustic Estimates of Zooplankton Biomass,'' ICES J. Mar. Sci. **51**, 505–512.

Turin, G. L. (**1960**). ''An Introduction to Matched Filters,'' IRE Trans. Inf. Theory **IT-6(3)**, 311–329.

Wiebe, P. H., Mountain, D., Stanton, T. K., Greene, C., Lough, G., Kaartvedt, S., Manning, J., Dawson, J., and Copley, N. (**1996**). ''Acoustical Study of the Spatial Distribution of Plankton on Georges Bank and the Relationship Between Volume Backscattering Strength and the Taxonomic Composition of the Plankton,'' Deep-Sea Res. II **43**, 1971–2001.

Winder, A., and Loda, C. J. (**1981**). *Space-time Information Processing* (Peninsula, Los Altos, CA), pp. 153–156.